Supplementary Information

Design of Lithium Disilicate Glass-Ceramic Based Highly Thermally Stable LuAG :Ce PiG Green Converter for Dynamic Laser Illumination

Yusai Xu [a]， Qianxiong Wen [a], Xidong Wang [b], Cong Zhao [b], Enrou Mei [a], Meilin Fu [a], Teng fei Tian [a], Xiaojuan Liang [a]*, Wenxia Gao [a]*, Weidong Xiang [a]*

a College of Chemistry and Materials Engineering, Wenzhou University, Wenzhou, 325035, China

b College of Life and Environmental Science, Wenzhou University, Wenzhou 325035, China

** Corresponding Authors:*

Email:lxj6126@126.com, gaowenxia@cdu.edu.cn, wzuxwd001@126.com

1. Experimental Section

1.1 Raw materials

The raw materials used in this study are all commercially available high-purity materials. Commercial LuAG: Ce phosphor (wavelength 520 nm) was purchased from Hangzhou Fluorescent New Materials Co. Silicon dioxide (SiO_2), lithium carbonate (Li_2CO_3), magnesium oxide (MgO), boron trioxide (B_2O_3), zirconium dioxide (ZrO_2), calcium oxide (CaO), and sodium carbonate (Na_2CO_3) were purchased from Aladdin Biochemical Technology Co. Aluminum trioxide (Al_2O_3), phosphorus pentoxide (P_2O_5) and potassium carbonate (K_2CO_3) were purchased from Shanghai Myriad Biochemical Technology Co. The purity was 99.99%. The raw materials are used directly without subsequent processing.

1.2 Selective preparation of precursor glass matrix and sintering of LDGC-LuAG PiG

An excellent glass system has a decisive impact on the thermal stability, optical properties, chemical stability, and applications of PiG. In recent years, LDGC has been widely utilized in various fields including dental restorative materials,

mechanical manufacturing, optics, electronics, and microelectronics, as well as aerospace and aviation due to its exceptional chemical resistance and elevated mechanical strength. Moreover, LDGC offers excellent thermal stability and moderate semi-permeability for suitable applications, which makes it extremely desirable for use in fluorescent color converters. The long-term stability of PiG can be maintained by employing LDGC during the preparation process to enhance its resistance against certain levels of chemical corrosion. Additionally, the prepared PiG reduces the risk of cracks or structural changes caused by temperature variations due to its moderate coefficient of thermal expansion. By utilizing LDGC with appropriate ratios, superior optical transparency can be achieved facilitating efficient transmission and radiation of phosphor. In this paper, we innovatively prepared a novel LDGC as a precursor material for LuAG PiG using compositional molar ratios SiO_2-Li_2O-Al_2O_3-P_2O_5-K_2O-MgO-B_2O_3-ZrO_2-CaO-Na_2O (60.35%-25.15%-1.00%-2.00% - 1.50% - 2.00% - 2.50% - 2.50% - 1.00%-2.00%). To ensure optimal mechanical properties of the LDGC design was made with a SiO_2 to Li_2O molar ratio set at 2.4 while P_2O_5 and ZrO_2 were added as nucleating agents for the glass along with Na_2O, K_2O, and additional components to lower melting temperature. Finally, the various glass components were mixed in stoichiometric ratios. The mixed powder was thoroughly ground in a mortar before being poured into an adamantine crucible and melted in a muffle furnace at 1400°C for 1 hour. Subsequently, the molten glass was quenched by pouring it into cold water to obtain lumpy glass, which was then dried in an oven. Finally, the dried glass underwent ball milling for 5 hours and sieving to obtain lithium disilicate microcrystalline glass-ceramic precursor powders with a particle size of 50 μm. The one-step low-temperature co-sintering preparation process of LDGC-LuAG PiG is illustrated in Figure S2. Thorough and uniform mixing of the resulting glass powder with commercial LuAG phosphor took place in an onyx mortar, followed by sintering in a muffle furnace at temperatures ranging from 800°C to 880°C for 30 minutes to ultimately prepare LDGC-LuAG PiG Immediately after preparation, the LDGC-LuAG PiG samples were precisely cut using a commercial cutter and polished into square pieces measuring 10*10*1 mm^3 for subsequent characterization and laser

testing.

1.3 Characterization

Crystalline phase identification and micro-morphological characterization The crystalline phase composition and crystal structure of the samples were tested by x-ray powder diffraction (D8 Advance, Bruker, Germany) with a current of 40 mA, a voltage of 40 mV, and a test angle (2θ) of 10°-80°. A phosphor microscope (DM13000B, Germany) was used to photograph the distribution of phosphors on the surface of the samples and the luminescence morphology on the nanometer scale. The morphology of the samples was analyzed using a field emission scanning electron microscope (Zeiss Sigma 300) to obtain a uniform distribution of the phosphors in the glass matrix, and the elemental distribution in the samples was obtained by EDS analysis (Bruker Quantax XFlash SDD 6 | 30 Esprit 2.0). High-throughput, high-resolution chemical characterization and dynamic observation of the samples were carried out by a high-resolution transmission electron microscope (Talos F200S G2 S/TEM), TEM magnification range: 25-105 million times, line resolution: ≤ 0.10 nm, maximum accelerating voltage: 200 kV, and maximum angle of convergence of LACBED: ≥ 100 [mrad], and ultimately, a high-definition The sample surface morphology, the homogeneous wrapping of the phosphor by the glass matrix, and a variety of clear and obvious lattice stripes were obtained.

Measurement of physical properties and luminescence characteristics The pristine glass powder samples were subjected to differential scanning calorimetric analysis (DSC, HCT-4, HENVEN, Beijing), revealing the presence of three distinct heat absorption peaks in the temperature range of 0 °C to 1000 °C. These peaks corresponded to the glass transition temperature T_g (480 °C), crystallization temperature T_P^1 (741 °C), and crystallization temperature T_P^2 (888 °C). PLE spectra and PL spectra were measured using a phosphor spectrometer ((FLS920), Edinburgh). The transmittance of the samples within the wavelength range of 300-800 nm was determined using a UV-Vis spectrophotometer (Shimadzu UV-2550, Japan). Internal and external quantum efficiency as well as absorbance data for different

concentrations of both samples and phosphors were obtained using a UV-NIR absolute quantum yield meter (Quantaurus-QY Plus C13534-12, Hamamatsu Photonics). Thermal stability was assessed utilizing a fiber optic spectrometer (NOVA extreme-sensitivity spectrometer, idea optics, China) by measuring temperature-dependent PL spectra for both samples and relative phosphor intensities between pristine phosphor and LDGC-LuAG PiG. Phosphor decay curves were acquired through a UV-visible near-infrared phosphor test system (FLS980, Edinburgh). Additionally, thermal conductivity and thermal diffusion coefficient measurements were conducted on LDGC-LuAG PiG employing a thermal conductivity meter (LFA470, Netzsch, Germany). Luminescence characteristics including LE, CIE, CCT, CRI, LF, and luminescence power density were evaluated via transmission laser(MCPD-9800) with an optical detection device comprising high-power blue laser emitter at 450 nm wavelength, multichannel spectrometer (F-4600，Hitachi，Chengdu，Japan)，and integrating sphere. The optical detection device consisted of the following components: a high-power blue laser emitter with a wavelength of 450 nm, a multichannel spectrometer (F-4600, Hitachi, Chengdu, Japan), and an integrating sphere (PMS-50, Everfine, Hangzhou, China). The current, power, spot area, and power density of the high-power blue laser source were 0.06-3.0 A, 0.565-54.2 W, 1.21 mm^2, and 0.47-44.79 $W\text{-}mm^{-2}$, respectively.

Supplementary Figures

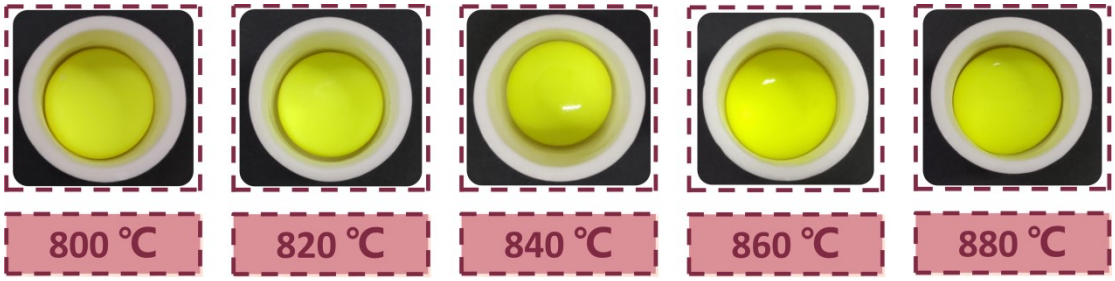

Figure S1. 30% wt% LDGC-LuAG PiG sample photo after sintering at different temperatures.

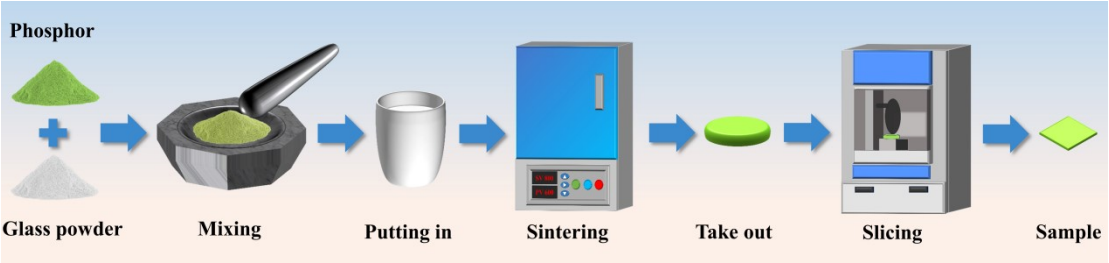

Figure S2. Preparation process of LDGC-LuAG PiG.

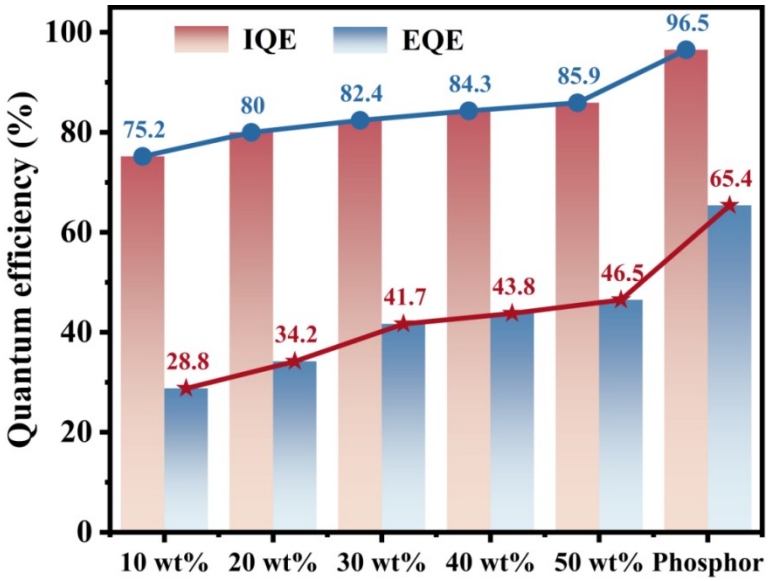

Figure S3. Comparison of quantum efficiency of LDGC-LuAG PiG with raw phosphor at different concentrations.

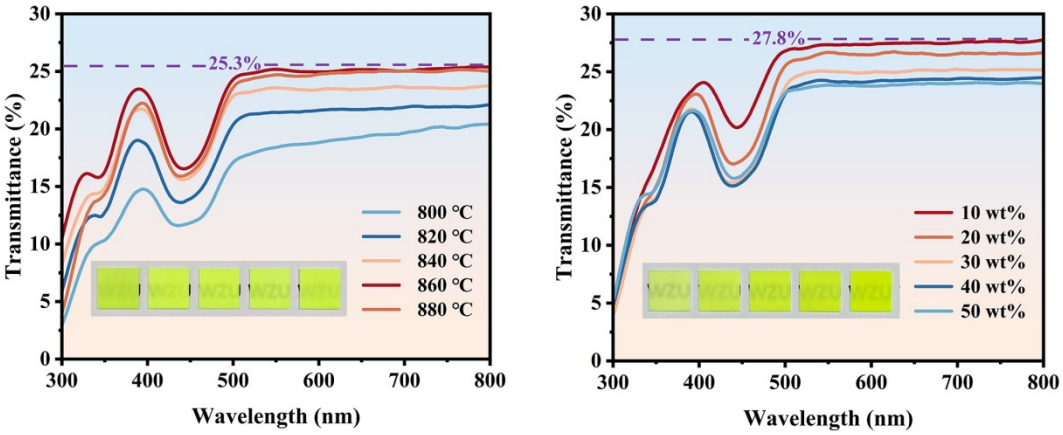

Figure S4. Temperature gradient and concentration gradient transmittance.

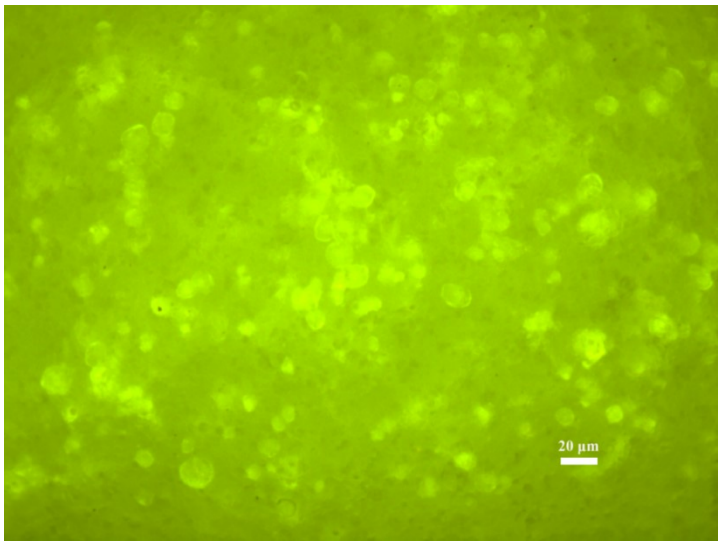

Figure S5. phosphor microscope appearance of LDGC-LuAG PiG.

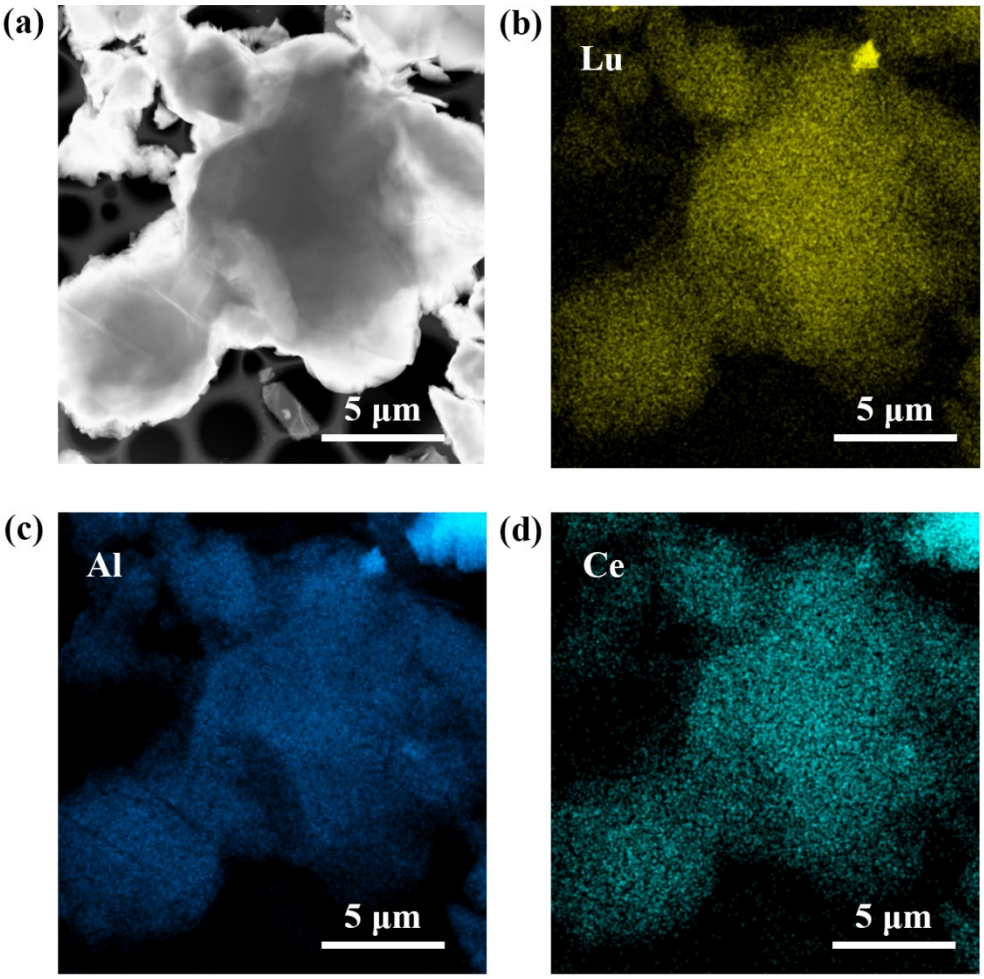

Figure S6. EDS mapping pictures of the LDGC-LuAG PiG.

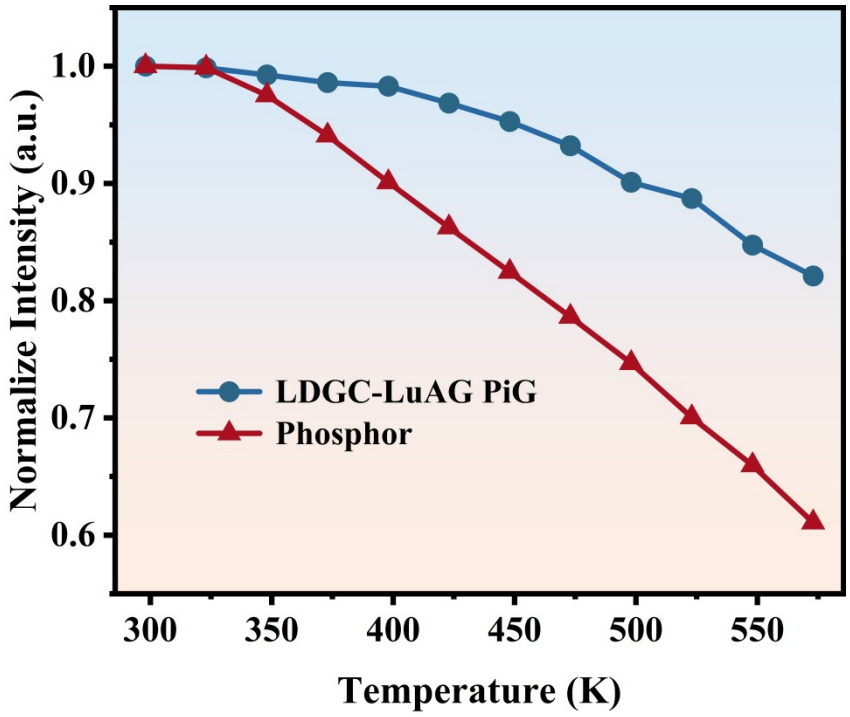

Figure S7. Comparison of the relative intensity of temperature-dependent tests for LDGC-LuAG PiG and LuAG phosphor.

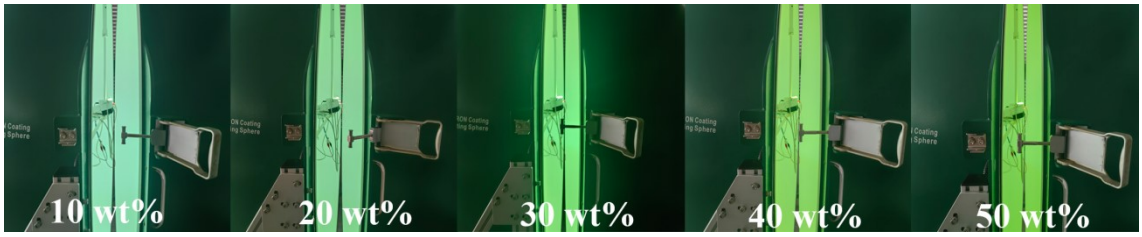

Figure S8. Laser test spotting diagrams for different concentrations of LDGC-LuAG PiG.

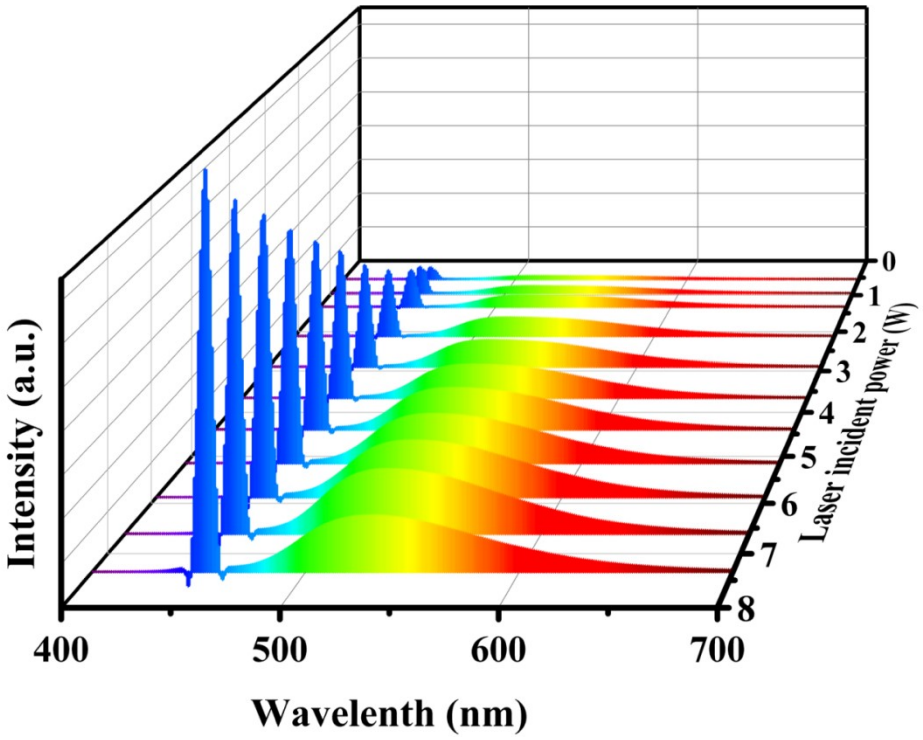

Figure S9. EL spectra of 20 wt% LDGC-LuAG PiG at different powers

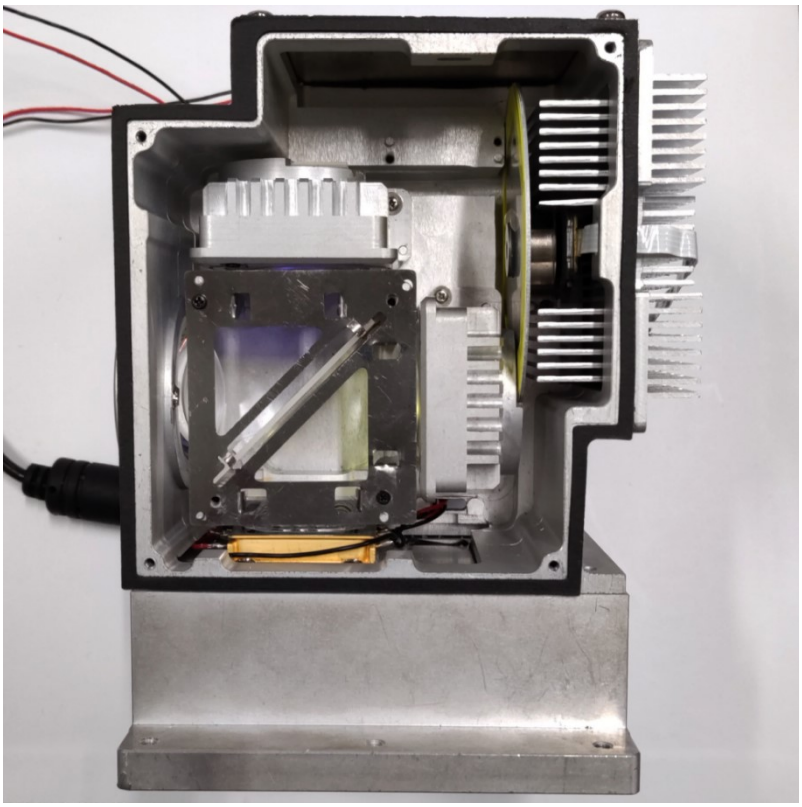

Figure S10.Commercial laser lighting dynamic module internal structure

Table.S1 Absorption efficiency and quantum efficiency of 10-50 wt% LDGC-LuAG PiG, Phosphor.

	Absorption efficiency	**EQE**	**IQE**
10 wt%	38.4%	28.8%	75.2%
20 wt%	42.8%	34.2%	79.9%
30 wt%	50.7%	41.7%	82.4%
40 wt%	52.7%	43.8%	84.3%
50 wt%	54.2%	46.5%	85.9%
Phosphor	67.8%	65.4%	96.4%

Table.S2 Laser performance of LDGC-LuAG PiG with different concentration in this work.

Samples	SP(W)	ST(Wmm^{-2})	LF(lm)	LE(lm/W)	CCT(K)	CRI	CE(%)
10 wt%	5.15	7.23	1021.4	228.78	7068	68.1	58.10
20 wt%	7.34	10.6	1584.3	246.20	7431	58.4	61.40
30 wt%	6.25	8.89	1268.1	227.49	9665	54.3	64.60
40 wt%	6.61	9.46	1240.9	224.13	6060	53.9	55.10
50 wt%	4.77	6.66	869.03	209.82	6419	50.3	57.30

Table.S3. Laser power corresponds to the laser power density in the laser test

Laser power (W)	Laser power density (W/mm^2)
0.54	0.5303
0.75	0.81818
0.94	1.13636
1.134	1.42424
1.322	1.71818
1.717	2.00303
2.112	2.60152
2.494	3.2
2.889	3.77879
3.28	4.37727
3.658	4.9697
4.032	5.54242
4.397	6.10909
4.774	6.66212
5.147	7.23333
5.51	7.79848
5.873	8.34848

6.248	8.89848
6.611	9.46667
7.221	10.01667
7.343	10.6

Table

Notes in Tables:

SP: Saturation power

ST: Saturation power density

LF: Luminous flux

LE: Luminous efficiency

IQE: Internal quantum efficiency

EQE: External quantum efficiency

CCT: Correlated color temperature

CRI: Color rendering index

CE: Conversion efficiency